Nanoscale

Accepted Manuscript

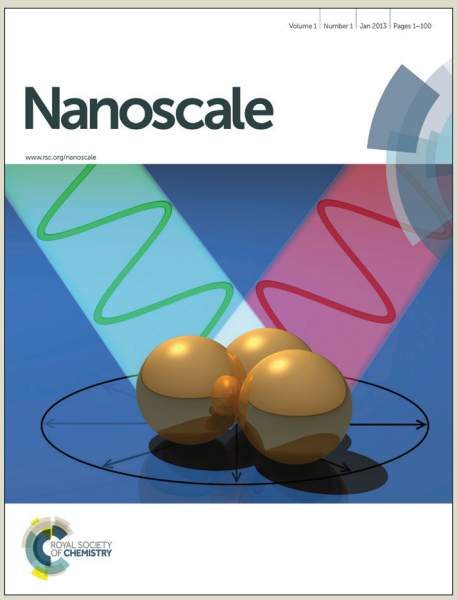

This is an *Accepted Manuscript*, which has been through the Royal Society of Chemistry peer review process and has been accepted for publication.

Accepted Manuscripts are published online shortly after acceptance, before technical editing, formatting and proof reading. Using this free service, authors can make their results available to the community, in citable form, before we publish the edited article. We will replace this *Accepted Manuscript* with the edited and formatted *Advance Article* as soon as it is available.

You can find more information about *Accepted Manuscripts* in the Information for Authors.

Please note that technical editing may introduce minor changes to the text and/or graphics, which may alter content. The journal's standard Terms & Conditions and the Ethical guidelines still apply. In no event shall the Royal Society of Chemistry be held responsible for any errors or omissions in this *Accepted Manuscript* or any consequences arising from the use of any information it contains.

ROYAL SOCIETY OF CHEMISTRY

www.rsc.org/nanoscale

Nanoscale

RSCPublishing

ARTICLE

Thermal Conductivity Measurements of High and Low Thermal Conductivity Films Using a Scanning Hot Probe Method in the 3ω Mode and Novel Calibration Strategies

Cite this: DOI: 10.1039/xoxxoooooox

Received 22nd January 2015,
Accepted ooth January 2012

DOI: 10.1039/xoxxoooooox

www.rsc.org/nanoscale

Adam A. Wilson,[a*] Miguel Muñoz Rojo, [b*] Begoña Abad Mayor, [b] Jaime Andrés Perez, [b] Jon Maiz, [b] Jason Schomacker [a], Marisol Martín Gonzalez, [b] Diana Andra Borca-Tasciuc [a] and Theodorian Borca-Tasciuc[a†]

*These authors contributed equally to this work

This work discusses measurement of thermal conductivity (k) of films using a scanning hot probe method in the 3ω mode and investigates the calibration of thermal contact parameters, specifically the thermal contact resistance (R_C^{th}) and thermal exchange radius (b) using reference samples with different thermal conductivities. R_C^{th} and b were found to have constant values (with $b = 2.8 \pm 0.3\ \mu m$ and $R_C^{th} = 44{,}927 \pm 7820 \frac{K}{W}$) for samples with thermal conductivity values ranging from 0.36 W/K·m to 1.1 W/K·m. An independent strategy for the calibration of contact parameters was developed and validated for samples in this range of thermal conductivity, using a reference sample with previously measured Seebeck coefficient and thermal conductivity. The results were found to agree with the calibration performed using multiple samples of known thermal conductivity between 0.36 and 1.1 W/K·m. However, for samples in the range between 16.2 W/K·m and 53.7 W/K·m, calibration experiments showed the contact parameters to have considerably different values: $R_C^{th} = 40{,}191 \pm 1532 \frac{K}{W}$ and $b = 428 \pm 24\ nm$. Finally, this work demonstrates that using these calibration procedures, measurements of both highly conductive and thermally insulating films on substrates can be performed, as the measured values obtained were within 1-20% (for low k) and 5-31% (for high k) of independent measurements and/or literature reports. Thermal conductivity results are presented for SiGe film on glass substrate, Te film on glass substrate, polymer films (doped with Fe nano-particles and undoped) on glass substrate, and Au film on Si substrate.

1. Introduction

Measurement of thermal conductivity of films, bulk materials and nano-structured materials is of paramount importance in several applications. Among them are waste-heat management in microelectronics, and efficiency of solid-state energy conversion in thermoelectric materials[1–4]. Thus, thermal characterization techniques that allow for fast, consistent, versatile measurements of nano-structured materials, thin-films, and bulk materials are of great need. In recent decades, methods have been developed to measure thermal conductivity of thin-films and bulk samples. These techniques include the time-dependent thermo-reflectance (TDTR) method[5], the photo-acoustic technique (PA)[6], the laser flash method[7], transient plane source (TPS) method[8], bridge techniques[9], and the photo-thermoelectric technique[10], among others. However, each of these techniques has its shortcomings: TDTR and PA require a metallic layer to be deposited on top of the sample to be investigated, which renders the sample more difficult to use for future measurements, and for these techniques, the spatial resolution is on the order of tens of micrometers, or larger, which prohibits investigations of nanostructures[5,6]; the laser flash and photo-thermoelectric methods do not allow for spatial characterization[7,10]; TPS uses a millimeter-sized heating source (which lessens the need to find thermal contact resistance, but which limits spatial resolution)[8]; and the bridge techniques require specially prepared samples, which are free-standing or semi-free-standing in order to perform the measurements [9].

However, Scanning Thermal Microscopy (SThM) using heated micro probes, which has been successfully employed to measure the thermal conductivity of films[11] and nanowires[12–14] , allows for relatively fast, repeatable experiments for a wide variety of sample types, does not require knowledge of the specific heat and density of the material, and requires minimal sample preparation. In this technique, an electrically

Nanoscale Accepted Manuscript

conductive tip is heated with a DC current, or, as in the case of this work, an AC current (with angular frequency ω) while it exchanges heat with the ambient and the surface of a sample. As the probe's electrical resistance depends on its temperature, the temperature change will induce a DC resistance change and an AC fluctuation. The temperature-induced resistance change varies with the second harmonic frequency, 2ω. This fluctuation in resistance will lead to a voltage rise in the third harmonic, (referred to in this work as $V_{3\omega}$), proportional to the 2ω AC temperature rise of the probe[15]. Both the DC and AC thermal response of the probe may be correlated with the thermal resistance of the probe, thermal contact resistance between probe and sample, and thermal resistance of the sample. For a given applied heating power to the probe, the rate of heat exchanged between the probe and the sample will change as a function of thermal conductivity of the sample, and thus the temperature of the probe will also vary; thus, by monitoring the probe's temperature (by way of recording the $V_{3\omega}$ signal), the sample's thermal properties may be obtained. Moreover, under AC heating, the Seebeck coefficient may be obtained by monitoring the DC temperature rise and DC Seebeck voltage across probe and sample[16].

Figure 1 shows the thermal interaction between the probe and sample. One of the major concerns when using this technique is the accurate determination of the thermal exchange radius, b, and the thermal contact resistance, R_C^{th}. Previous works using a scanning hot probe have assumed constant values for b and R_C^{th}[17–21], some making the assumption that all the heat is transferred from the probe to a single point on the sample[20,21], and others assuming that the heat transfer is contained within a disc at uniform temperature of radius b [17–19].

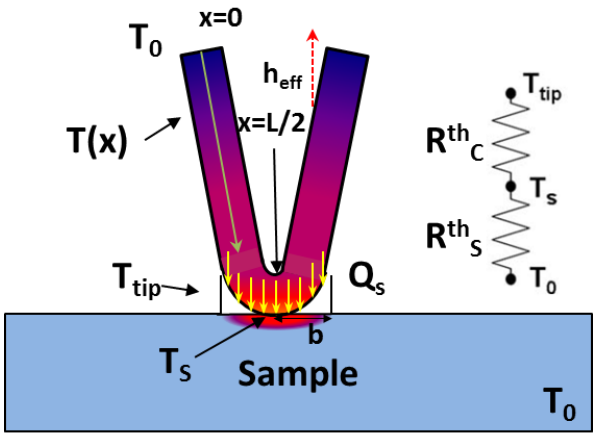

Figure 1 *– Schematic of thermal interaction between probe and sample, with thermal exchange radius, b, and thermal contact resistance,* R_C^{th}

In this work, we explore the dependence of the values of $\boldsymbol{R_C^{th}}$ and $\boldsymbol{b}$ on the thermal conductivity of the sample, validate probe calibration methods proposed in previous works[11,18], introduce an AC scanning probe method to find the Seebeck coefficient using 2ω Seebeck voltage and temperature from $\boldsymbol{V_{3\omega}}$, and propose a new method of probe calibration using a sample with known Seebeck coefficient and thermal conductivity. Finally, we use the appropriately calibrated probe to find the thermal conductivity of films of both low $\boldsymbol{k}$ (0.36-1.1 W/ K·m) and high $\boldsymbol{k}$ (above 16.2 W/ K·m).

2. Experimental

2.1 Obtaining thermal conductivity and Seebeck coefficient using 3ω–SThM.

For probe heating using DC current, (or AC current at low frequency, when the heat capacity effects are negligible, and temperature rise amplitude is frequency independent and equivalent to the DC temperature rise to good approximation) the governing equation describing the amplitude of the temperature profile of the probe shown in Fig. 1 is given by[11],

$$\frac{d^2T^*}{dx^2} - \left(\frac{2h_{eff}}{k_p r} - \frac{I^2\rho_0 TCR}{k_p\pi^2 r^4}\right)T^* + \frac{I^2\rho_0}{k_p\pi^2 r^4} = 0, \qquad (1)$$

where $T^* = T(x) - T_0$, $h_{eff} = h + 4\epsilon\sigma T_0^3$ (here, h is the convective heat transfer coefficient, ϵ is the probe's emissivity, and σ is the Stefan-Boltzmann constant), ρ_0 and k_p are the probe's electrical resistivity and thermal conductivity, respectively, TCR is the probe's temperature coefficient of resistance, I is the root-mean-square electrical current applied to the probe, and r is the radius of the probe. The contribution from radiation is negligible for probe operating temperature near ambient[15]. To obtain an analytical solution to the second order differential equation, two boundary conditions are employed. The first is an assumption that the ends of the probe are at ambient temperature (i.e. $T(0) = T_0$). The second assumes the tip region of the probe (of length 2b) is of uniform temperature, and by energy balance therein,

$$-k_p A\frac{dT^*}{dx}|_{x=L/2-b} + I^2\rho_0(1 + TCR \times T^*|_{x=L/2-b})\frac{b}{A} = \frac{Q_s}{2}, \qquad (2)$$

where the left-hand side is heat conduction and Joule heating of the probe, $A = \pi r^2$ is the probe's cross-sectional area, and L is the length of

Nanoscale Accepted Manuscript

 This journal is © The Royal Society of Chemistry 2015

the probe, and where the right-hand side is the heat transfer through one leg of the probe (thus half the total heat transfer to the sample, by symmetry). Finally, the heat transfer rate between probe and sample, Q_s, is given by

$$Q_s = \frac{\Delta T_{tip}}{R_C^{th}+R_S^{th}} = \frac{\Delta T_S}{R_S^{th}}, \quad (3)$$

where $\Delta T_{tip} = T_{tip} - T_0$ and $\Delta T_S = T_S - T_0$ are the temperature of the probe and sample, respectively, in the tip region, and R_S^{th} is the sample thermal resistance. Solving equation (1) to obtain the temperature profile along the probe for a given value of Q_s yields the following expression:

$$\Delta T_p(x) = C_1 e^{\lambda x} - C_2 e^{-\lambda x} + \frac{\Gamma}{\lambda^2}, \quad (4)$$

where $\lambda = \frac{I^2\rho_0}{k_p\pi^2r^4}$, $\Gamma = \frac{2h_{eff}}{k_p r} - \frac{I^2\rho_0 TCR}{k_p\pi^2r^4}$, and the constants C_1 and C_2 are easily obtained by applying the boundary conditions (eq. 2 and $T(0) = T_0$).

If the sample is bulk, or has bulk-like thickness, the thermal conductivity is found from R_S^{th} by employing the semi-infinite medium assumption and solving the expression for 2D bulk samples:

$$R_S^{th} = \frac{1}{4\kappa_{sample} b} \quad (5)$$

If the sample is a thin film on substrate, and is thin enough that there is negligible heat spreading in the in-plane directions of the sample, the thermal conductivity is found by solving the expression for the series thermal resistance across substrate and film, with 1D heat transfer across the thickness of the film:

$$R_S^{th} = \frac{1}{4\kappa_{substrate} b} + \frac{l}{\pi\kappa_{film} b^2} \quad (6)$$

where l is the film thickness[11].

When heat transfer in the film(s) may be multidimensional and anisotropic, models developed by Son *et. al.*[22] for laser heating may be used to predict thermal resistance of the sample, based on the film and substrate's respective values of thermal conductivity.

In order to determine the thermal resistance of the sample, the thermal resistance of the probe (R_P^{th}) must be experimentally obtained. To accomplish this, the $V_{1\omega}$ across both probe ($V_{1\omega,p}$) and the entire circuit, which typically consists of a series resistor and probe[11] ($V_{1\omega,tot}$), and the $V_{3\omega}$across the probe must be measured. Ultimately, R_P^{th} is calculated as described by Zhang *et. al.*[16] as the average temperature rise of the probe, $\Delta T_{probe,ave}$, divided by the RMS power ($V_{RMS} \times I_{RMS}$). The amplitude of the AC temperature rise of the probe is determined as $\Delta T_P = \frac{2V_{3\omega}}{TCR\, V_{1\omega,p}}$ [11,31], and the power is calculated as $P = I_{1\omega}^2 R_p$, where R_p is the electrical resistance of the probe at the calculated operating temperature. Here, the $V_{1\omega,p}$ signal was scaled to include only the probe section by removing the resistive voltage drop due to the electrical contact resistance with the external wires (~0.5 Ω in our experiment) Finally, the $V_{2\omega}$ Seebeck voltage between probe and sample is also measured, from which we obtain the Seebeck coefficient, as described later in the text. The experimental set-up consists of a high-accuracy resistor with resistance $R_{ref} = 10\ \Omega$ connected in series with a SThM probe. The probe is mounted in an AFM head. The AFM used is a commercial unit supplied by *Nanotec Electronica*® that works as nano-positioner, equipped with a probe mount designed in the lab for these tips. The SThM probe is a commercial probe from Bruker AFM®, which is a Wollaston wire, composed of an alloy of platinum (90%) and rhodium (10%) (*i.e.* Pt90/Rh10), clad with silver, except the thermally active region (of length around 200 μm) where the Pt90/Rh10 core is exposed[23]. Then, the electrical circuit is connected to an ultra-high-frequency lock-in amplifier from Zurich Instruments® that applies an AC current across the circuit and records $V_{1\omega}$ both across the probe and across the total circuit, $V_{2\omega}$ across the probe and sample, and $V_{3\omega}$ across the probe, simultaneously. This lock-in amplifier was used to allow for measurements to be performed at an operating frequency range of 5 Hz – 10 kHz. Figure 2 is a representative schematic of the experimental setup of the probe and sample system.

Nanoscale Accepted Manuscript

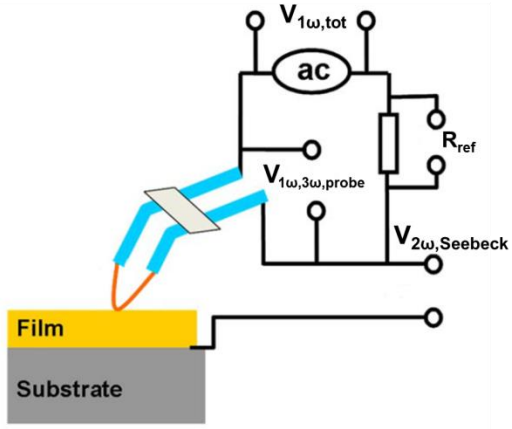

Figure 2 *– Representative Schematic of Experimental Set-up*

After obtaining R_P^{th}, R_S^{th} is calculated by fitting for the value of Q_S (eq. 3) between the probe and sample which matches R_P^{th} to the appropriate average probe temperature rise, which is obtained by averaging equation 4 over the length of the probe. Obtaining the probe's temperature in the tip region (i.e. when L/2-b≤x≤L/2), which by definition is constant, with value ΔT_{tip}, and dividing by Q_S gives the thermal resistance ($R_{tip}^{th} = R_S^{th} + R_C^{th}$) for the heat transfer from the tip through the sample (*i.e.* within the disc of constant temperature for uniform samples)[11,17]. Thus, if R_C^{th} is known, R_S^{th} is readily obtained.

In order to determine the magnitude of the Seebeck coefficient of the sample, the Seebeck voltage is obtained by scanning the surface of the sample in contact and measuring the amplitude of $V_{2\omega}$ between the probe and sample, averaging over the scanned area, and dividing by the temperature rise across the sample, and accounting for the contribution to the Seebeck voltage from the probe electrodes. In other words:

$$S_{sample} = (V_{2\omega} - S_{probe}\Delta T_{tip})/\Delta T_{sample} \qquad (7)$$

Note that because the temperature and voltage values used in this equation are amplitudes, the absolute value of the Seebeck coefficient is what is obtained by this method.

2.2 Probe calibration.

In the previous section, it was established that to obtain the sample thermal conductivity from the probe's thermal resistance, thermal exchange radius, b, and thermal contact resistance, R_C^{th} must be known. Also, the experimental data is contingent upon the probe's temperature coefficient of resistance (TCR). Additionally, heat losses to the ambient must be accounted for. Thus, proper calibration is needed to account for these parameters. To this end, methods to determine b and R_C^{th} were developed. One such method employs a patterned sample with regions of significantly different thermal conductivity (one with low thermal conductivity, around 1.5 W/mK, and the other with high thermal conductivity, around 150 W/mK), and with the probe in contact, the interface between the two regions is passed over and $V_{3\omega}$ measured. Due to the difference in thermal conductivity, the heat transferred to the sample will vary and thus $V_{3\omega}$ will vary, and half the distance the probe travels during the transition between the higher and lower values of $V_{3\omega}$ is taken to be the value for b[18]. This calibration technique does not account for R_C^{th}, so a separate calibration must be performed by measuring probe thermal resistance of a bulk sample with known thermal conductivity. Subtracting the intrinsic sample thermal resistance from the probe thermal resistance yields R_C^{th}[19]. However, this assumes that the thermal exchange radius is independent of sample thermal conductivity, which we show in this work to not be an accurate assumption over such a wide range of thermal conductivity values. Another method to determine b and R_C^{th} is to use experimental data taken from a pair of bulk samples with known thermal conductivity (and hence known sample thermal resistance, as we observe from equation 5) and take R_C^{th} to be a free parameter for each value of b[16]. A plot is then made of R_C^{th} vs. b for each sample, since these are the two unknowns in the analytical heat transfer model, and the location of the intersection between the graphs is taken to be the pair of values for R_C^{th} and b[11]. However, this method uses only one such intersection, and assumes that R_C^{th} and b are independent of sample thermal conductivity for a certain range of thermal conductivity values (between 0.1W/K·m and 2.0W/K·m[17]). To validate the assumption that R_C^{th} and b are constant in this range of thermal conductivity, we measured several samples with known thermal conductivity values within the presumed range of validity. If they are constant values, the plots of R_C^{th} vs. b would intersect at the same location. Alternatively, we propose an independent method of calibration, using only one sample, with known thermal conductivity and Seebeck coefficient, by using the analytical heat transfer model to find the pair of values of R_C^{th} and b which give rise to the correct thermal conductivity and Seebeck coefficient.

In order to obtain the appropriate values for h_{eff}, and in order to know the nominal electrical resistance of the probe, probe geometry must be obtained. To do this, SEM images were taken to calculate the length and diameter of the probe, and the electrical resistance of the probe was found by using the manufacturer specified value of electrical resistivity, ρ_0 for this probe, and letting $R_0 = \frac{\rho_0 L}{\pi r^2}$ (see explanation of this

Nanoscale Accepted Manuscript

 This journal is © The Royal Society of Chemistry 2015

process and figure S.1 in supporting information). Finally, h_{eff} is determined by finding the thermal resistance of the probe in air, with no sample present. This represents the case in which the heat flux between probe and sample is zero. Once the thermal resistance is determined and the value introduced to a heat transfer model, the h_{eff} parameter in the program is adjusted until the value of thermal resistance under no heat transfer to the sample matches what is observed experimentally. The manufacturer specifies the probe's TCR to be 0.00165 K^{-1}, which was confirmed by measuring the probe's electrical resistance as a function of temperature (see figure S.2 in supporting information), yielding the same result, within the margin of uncertainty. Table I contains the pertinent information regarding the probe.

Table I. *Probe properties and how they were determined*.

Parameter	**Value**	**How Obtained**
Length (L)	206.48μm	Experiment
Diameter ($d_p = 2r$)	4.96μm	Experiment
Thermal Conductivity (κ_p)	38.0 $Wm^{-1}K^{-1}$	Manufacturer specification
Probe-Air Heat Transfer Coefficient (h)	2363 $Wm^{-2}K^{-1}$	Experiment
Temperature Coefficient of Resistance (TCR)	0.00165 K^{-1}	Manufacturer specification /Experiment
Nominal Electrical Resistance (R_0)	2.185 Ω	Measured length/diameter and manufacturer specified electrical resistivity.

2.3 b and R_C^{th} determination from calibration sample measurements.

In this work, all the experiments were performed with room temperature at 28˚C and with 30% relative humidity. Before each measurement, the probe was verified, via an integrated optical camera, to be perpendicular to the plane of the sample. To verify that constant force was applied to the sample's surface when bringing the probe into contact, the contact set point voltage was kept at a constant value (5V). To calibrate the probe for low thermal conductivity measurements, the following samples with known thermal conductivities ranging from 0.36W/K·m and 1.1 W/K·m were measured: poly(3,4-ethylenedioxythiophene) (also known as PEDOT, with κ=0.36W/K·m), polyaniline (PANI) with 5% and 7% graphene nano-platelets (κ=0.49W/K·m and 0.65W/K·m, respectively)[24], p-type bulk Bi_2Te_3 (doped with Sb to ensure p-type formation) with κ=1.0 W/K·m, and borosilicate glass with κ=1.1 W/K·m. Also the following higher thermal conductivity reference samples were measured: AISI 304 steel (with κ=16.2 W/K·m) and 99.9% niobium from Goodfellow® (with κ=53.7 W/K·m). Calibration samples were prepared by cleaning and polishing each before measurement. Samples which were not chemically reactive with acetone (borosilicate glass, steel, and niobium) were cleaned by applying acetone to a cotton swab and gently daubing the sample. Polishing (for PEDOT, the PANI samples, and p-type Bi_2Te_3) was done by taking fine (1500) grit sand paper and gently grating across the sample's surface, and afterward was rubbed with a cloth and blown off to remove excess dust. Once prepared, the thermal resistance of each of these samples was measured at frequencies ranging 5 Hz to 1 kHz. For each sample, the measurement was repeated at three or more different locations to ensure repeatability, with variations of less than 1% observed. Figure 3a shows an exemplary graph of the average probe thermal resistance as a function of frequency. Note that the analysis in this work is taken from measurements performed within the range of frequency independent data (≤ 30 Hz). Figure 3b shows the average probe thermal resistance plotted against sample thermal conductivity of the reference samples at frequency of 10 Hz. Note that there is a region where the probe thermal resistance is very sensitive to changes in sample thermal conductivity, when thermal conductivity is below 2.0 W/K·m, whereas probe thermal resistance shows less sensitivity at higher values of sample thermal conductivity.

Nanoscale Accepted Manuscript

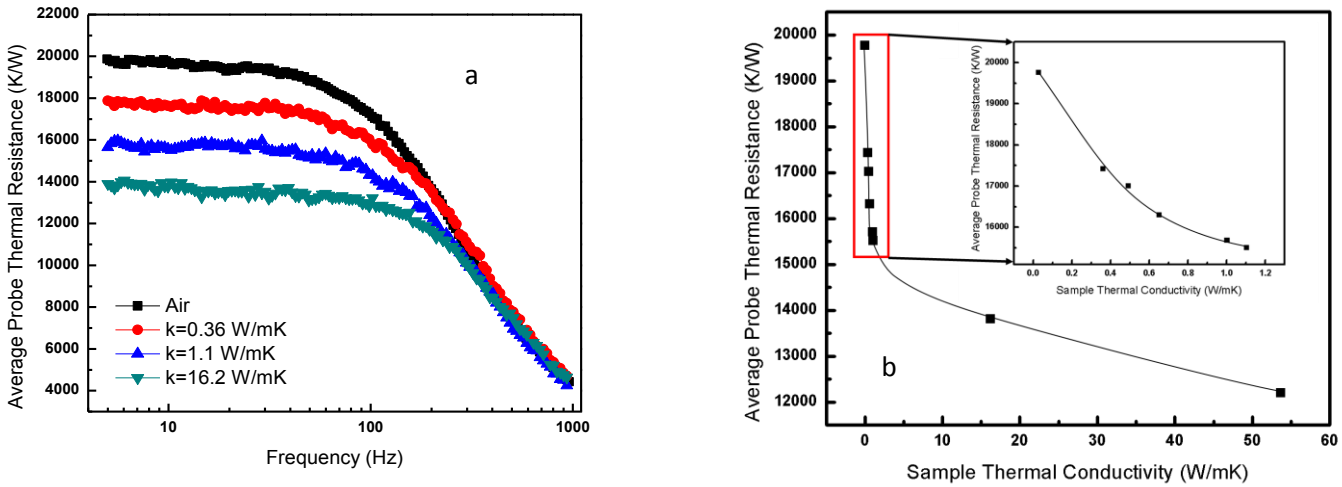

Figure 3 *– a)(left)Exemplary graph of measured average probe thermal resistance vs. frequency. Note that the average probe thermal resistance is independent of frequency below ~30 Hz. b)(right)Average probe thermal resistance vs. thermal conductivity of calibration samples. The inset shows the average probe thermal resistance vs. thermal conductivity of the calibration samples of low thermal conductivity (≤1.1 W/K·m).*

To describe the observed behaviour of the probe thermal resistance as a function of frequency, recall that the probe thermal resistance is directly proportional to the temperature, which varies directly with $V_{3\omega}$, which has been shown to decrease sharply above a certain "cut-off frequency", ω_C, which is limited by the thermal response time of the probe and/or applied signal amplification, which leads the average probe temperature to be inversely proportional to the frequency[19,20], leading to the behaviour reported here. Previous investigations have shown that $\omega_c \lesssim 1$ kHz[19], and has been shown to be even lower (~200 Hz) for the Wollaston probes used in this work[30]. Note that in this work, the data is taken from the frequency independent part of the signal that is not affected by the heat capacity of the sample or the probe and corresponds to an AC temperature amplitude equal to the DC temperature rise. Therefore, this system may not be used in the same way as the classical hot strip 3ω method, which employs the frequency dependent signal from a much faster heater/thermistor strip[19,31].

Among the calibration samples measured, five had values of thermal conductivity which fell between 0.36 and 1.1 W/K·m, where R_C^{th} and b are thought to be independent of sample thermal conductivity. To explore the validity of this assumption, R_C^{th} vs. b was plotted for each sample. Figure 4 shows this result. Note that the curves intersect at $b = 2.8 \pm 0.3\ \mu m$ and this corresponds to $R_C^{th} = 44{,}927 \pm 7820 \frac{K}{W}$. This supports the assumption that R_C^{th} and b remain constant for low thermal conductivity samples.

Nanoscale Accepted Manuscript

 This journal is © The Royal Society of Chemistry 2015

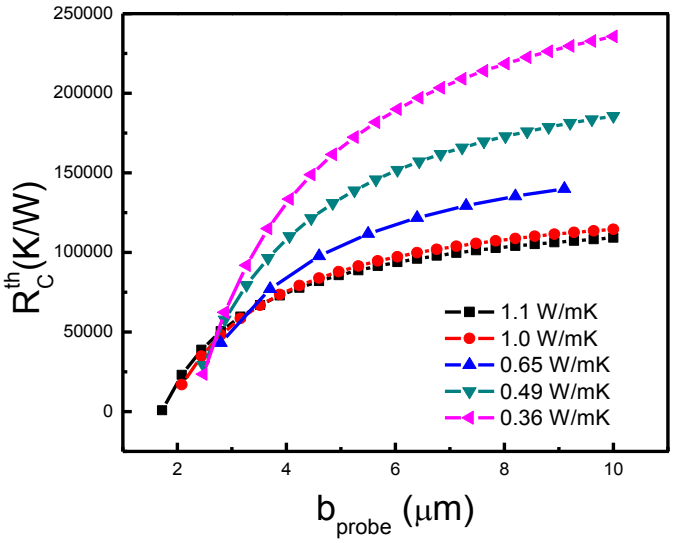

Figure 4 *- R_C^{th} vs. b for several calibration samples with thermal conductivity between 0.1 and 2.5 W/K·m. Curves intersect around the same point, giving confirmation to prior work only using two graphs.*

An independent method of calibration yielding similar results would further confirm the validity of the assumption that R_C^{th} and b remain constant for low thermal conductivity samples. To this end, a sample with known Seebeck coefficient and thermal conductivity (Sb-doped p-type Bi_2Te_3, with κ=1.0 W/K·m and S=172 ± 11 μV/K, as measured by the Seebeck Microprobe technique[26]) was scanned and the absolute value of the Seebeck voltage was measured at different locations, and averaged. Figure S.3 (found in the ESI) shows a histogram of voltage magnitude and the average value. The calculated Seebeck coefficient (see curve labeled "S-Calculated" in figure 5, obtained using Eqn. 7) is the ratio between the average Seebeck voltage and the calculated sample temperature rise, ΔT_S, from equation 3. Note that ΔT_S is found by matching the experimental probe thermal resistance to the calculated value from equations 2-5 for each value of b and corresponding R_C^{th} (see curve labeled "R_C^{th} vs b" in figure 5). In figure 5, the "S-Calculated" curve shows the result of this calculation as a function of b. The intersection with the horizontal line depicting the expected value of S (labeled "Expected S") is taken to be the calibrated b. Then, from the "R_C^{th} vs b" curve, the calibrated R_C^{th} is found at that value of b, which yields $b=2.84\pm0.16\mu m$ and $R_C^{th} = 47{,}924 \pm 4890\ K/W$. More information on how the Seebeck coefficient is obtained for this sample may be found in the ESI.

Nanoscale Accepted Manuscript

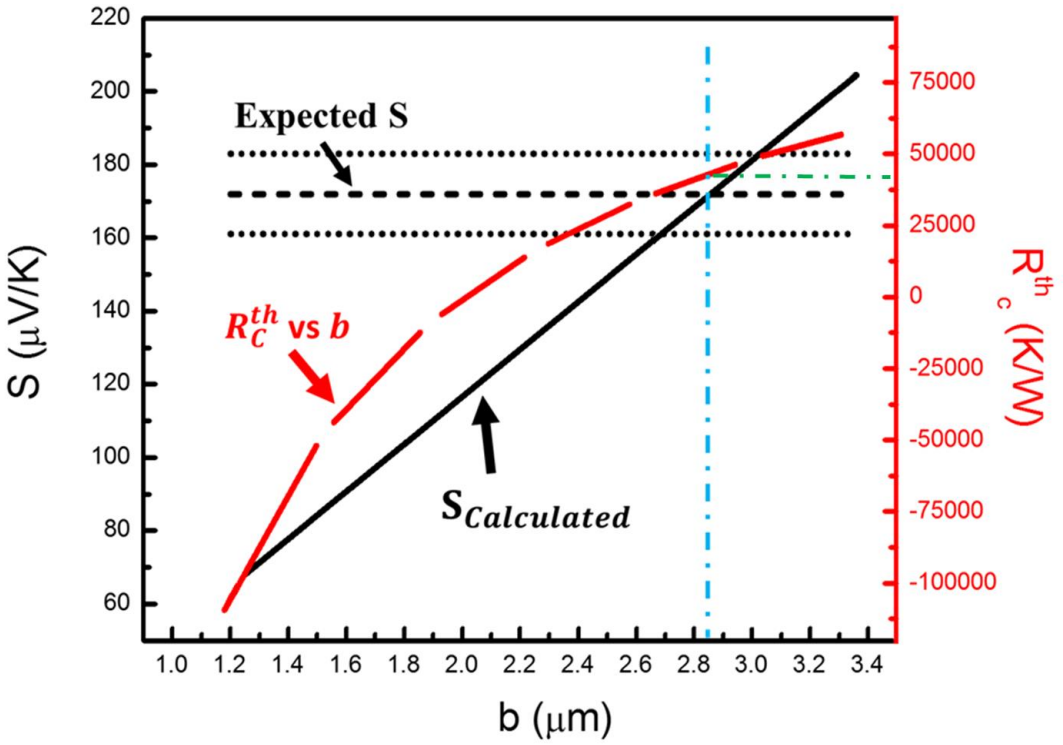

Figure 5 *– Seebeck Coefficient and R_C^{th} vs. b for p-type Bi_2Te_3, comparing with independently measured Seebeck Coefficient*

Thus, with the values of R_C^{th} and b well established, the technique may be used to find the thermal resistance of samples whose thermal conductivity is below or close to 1.1 W/K·m. However, if the thermal conductivity is well outside of this region, we must investigate calibration using higher thermal conductivity samples. To exemplify this, the thermal resistance of bulk samples of steel and niobium were measured, and if we assume that R_C^{th} and b are the same value as for the low thermal conductivity region, we obtain values of 3.87 W/K·m and 213.06 W/K·m, respectively, for their thermal conductivity, when the reference values of thermal conductivity are 16.2 W/K·m and 53.7 W/K·m, respectively. However, since the thermal conductivity is known for these two samples, if we plot R_C^{th} vs. b for steel and niobium, we find a new intersection, shown in figure 6, by which we obtain $R_C^{th} = 40{,}191 \pm 1532\frac{K}{W}$ and $b = 428 \pm 24nm$, which are taken to be more appropriate calibration values in this range of thermal conductivity.

Nanoscale Accepted Manuscript

This journal is © The Royal Society of Chemistry 2015

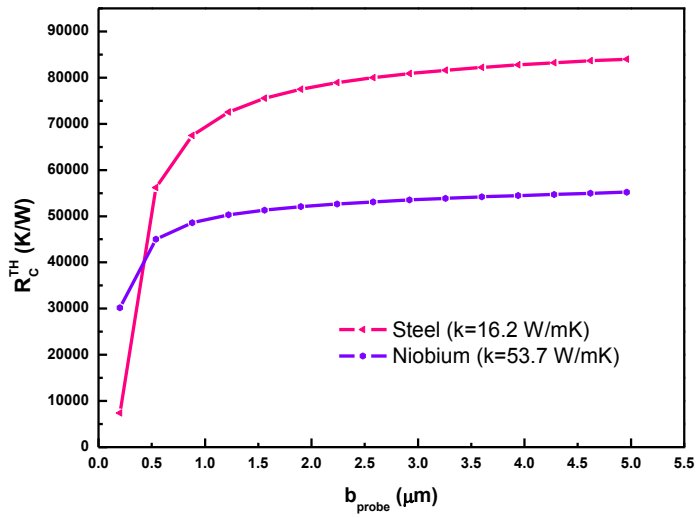

Figure 6 *- R_C^{th} vs. b for steel (κ=16.2 W/K·m) and niobium (κ=53.7 W/K·m) yielding a slightly lower value of R_C^{th}(40,191±1532 K/W) and a much lower value of b (428±24nm).*

2.4 Thermal conductivity measurements of films.

To test the validity of the results of calibration, and to demonstrate the use of this technique for measurement of thermoelectric systems, measurements of both the low thermal conductivity and high thermal conductivity films were performed. Many are well characterized in literature or measured by an independent method (see table 2). Figure 7 shows a representative schematic of the film samples measured.

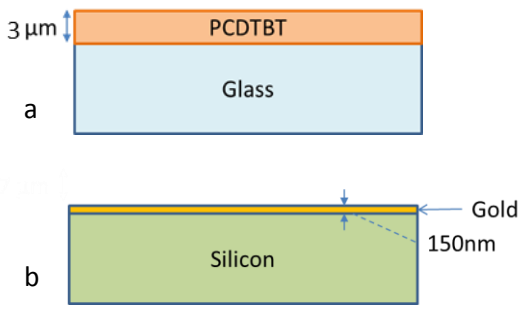

Figure 7 *– Representative schematic of film samples measured. Top (a): Low thermal conductivity films (for which thermal contact parameters are taken to be $R_C^{th} = 44{,}927 \pm 7820\frac{K}{W}$ and $b = 2.8 \pm 0.3$ μm), represented here by a 3 μm thick PCDTBT film on glass. Bottom (b): Gold film of thickness 150nm on silicon substrate, for which thermal contact parameters are taken to be R_C^{th}= 40,191±1532 K/W and b 428±24nm.*

Several samples with low thermal conductivity (between 0.1 and 1.3 W/K·m) were measured. They include: a polymer film, namely poly[N-9''-hepta-decanyl-2,7-carbazole-alt-5,5-(4',7'-di-2-thienyl-2',1',3'-benzothiadiazole)] (PCDTBT) without dopant, and another doped with Fe-nano-particles at a one-to-one dopant-to-polymer ratio, both with thickness of 3.0 μm, a tellurium film of thickness 2.74 μm, and a silicon-germanium film of thickness 1.8 μm. The PCDTBT (both doped and undoped) sample were prepared by drop-casting to a glass substrate. The thermal conductivity of the undoped sample was measured by PA to be 0.2±0.02 W/K·m. The Te film was prepared by electrodeposition to a glass substrate, and was found by PA to have a thermal conductivity of 0.78±0.08 W/K·m[27]. The SiGe film was prepared by metal-induced crystallization, and was grown on a glass substrate. A thermal treatment was applied ex-situ to the sample, and was measured by PA to have thermal conductivity of 1.23±0.12 W/K·m. The values of these films measured in this work were within 1-20% of the results obtained using PA, and are summarized in Table 2. The sample measured to test the higher thermal conductivity calibrations was thin-film gold (150nm) on a silicon substrate, whose value, as reported in literature under similar preparation conditions, was 150 W/mK[28]. In this case, as well as for the SiGe sample whose thickness was small enough for the substrate to have a non-negligible effect on the overall sample thermal resistance, COMSOL Multiphysic® simulations show that there is non-negligible in-plane heat spreading in the film (see Figure S.4 in ESI). Thus, to obtain the thermal conductivity of the film, a two-dimensional analytical model of heat transfer across a multi-layered thin-film sample was developed, being adapted from a Gaussian laser heating model [22,28]. In order to find the appropriate correlation between the *b* used in this work

Nanoscale Accepted Manuscript

and that of the radius of the Gaussian distribution, b_G, a model was developed in Solidworks®[32] to find the appropriate b_G by obtaining thermal resistance from the Gaussian distribution heat flux and adjusting b_G until the thermal resistance matched that obtained experimentally (using the disc constant temperature assumption). This was done for both bulk and multi-layered samples at various values of thermal conductivity, and it was found that if the value of thermal conductivity of the substrate was comparable to that of the film, taking the average temperature across the in-plane direction to the value of b_G yielded a one-to-one correlation with b. Once the correlation was established, the thermal resistance of the sample was matched to that predicted by the multilayer model by varying the film's thermal conductivity.

Table 2. *Sample measurements in high and low thermal conductivity regions, with the thickness of each sample, the thermal exchange radius used, the average probe thermal resistance, thermal contact resistance, sample thermal resistance and thermal conductivity, as well as expected value of thermal conductivity, if applicable (either independently measured, or reported in literature[27,29]).*

Sample	l	b	R_P^{th}	R_C^{th}	R_S^{th}	κ_{film}, **this work // ** κ_{film}, **expected**
SiGe film on glass substrate	1.8 µm	2.8±0.3 µm	14,948±54 K/W	44,927±7820 K/W	76,134±9494 K/W	1.22±0.21 W/K·m // 1.23±0.12 W/K·m
Fe-doped PCDTBT (1:1 doping concentration)	3.0 µm	2.8±0.3 µm	15,220±155 K/W	44,927±7820 K/W	87,022±14,631 K/W	1.03±0.15 W/K·m // (no data reported in literature)
PCDTBT (non-doped)	3.0 µm	2.8±0.3 µm	17,866±204 K/W	44,927±7820 K/W	358,859±66,204 K/W	0.25±0.04 W/K·m //0.20±0.02 W/K·m
Tellurium Film	2.74 µm	2.8±0.3 µm	15,749±75.5 K/W	44,927±7820 K/W	112,476±6,480 K/W	0.79±0.04 W/K·m //0.78±0.08 W/K·m
Au film on silicon substrate	150 nm	428nm±24nm	11,624±157 K/W	40,191±1532 K/W	5505±253 K/W	104.2±67.4W/K·m //110±2 W/ K·m
PEDOT [CAL]	Bulk	2.8±0.3 µm	17,429±217 K/W	44,927±7820 K/W	241,732±37,672 K/W	0.37±0.05 W/K·m // 0.36 W/K·m
PANI-5%GNP [CAL]	Bulk	2.8±0.3 µm	17,018±115 K/W	44,927±7820 K/W	188,595±27,836 K/W	0.47±0.06 W/K·m // 0.49 W/K·m
PANI-7%GNP [CAL]	Bulk	2.8±0.3 µm	16,314±118 K/W	44,927±7820 K/W	131,760±25,913 K/W	0.68±0.08 W/K·m //0.65 W/ K·m
p-type Bi_2Te_3 [CAL]	Bulk	2.8±0.3 µm	15,700±145 K/W	44,927±7820 K/W	92,113±11,911 K/W	0.97±0.11 W/K·m // 1.0 W/K·m
Borosilicate Glass [CAL]	Bulk	2.8±0.3 µm	15,516±134 K/W	44,927±7820 K/W	82,313±9787 K/W	1.08±0.11 W/K·m // 1.1 W/K·m
AISI 304 Steel [CAL]	Bulk	428nm±24nm	13,811±119 K/W	40,191±1532 K/W	37,511±3511 K/W	15.6±2.2 W/K·m // 16.2 W/K·m
Goodfellow® 99.9%pure Niobium [CAL]	Bulk	428nm±24nm	12,194±140 K/W	40,191±1532 K/W	10,632±2329 K/W	54.9±8.9 W/K·m // 53.7 W/K·m

[CAL] = Calibration Sample

Note the high uncertainty in the measurement of the thin-film Au on Si substrate. This is likely due to the fact that at the thermal resistance of the sample (both film and substrate) is only about 14% of the value of thermal contact resistance. Such a measurement demonstrates the

Nanoscale Accepted Manuscript

 This journal is © The Royal Society of Chemistry 2015

type of high thermal conductivity films where the calibration of thermal contact parameters have to be done using high thermal conductivity samples to obtain the expected result within the margin of uncertainty. The limitations of the method begin to be seen with measurement of high thermal conductivity materials such as this film-on-substrate measurement, as the thermal contact resistance is the main contributing factor to the overall thermal resistance measured by the probe[29]. Also, note that the value of the thermal conductivity of the gold on silicon film is very similar to that of the silicon substrate (whose thermal conductivity is nominally 148 W/mK). It is possible that the 2D film-on-substrate model predicted the correct film thermal conductivity in this case due to the fact that the film and substrate had comparable values of thermal conductivity. To verify the validity of the measurement of the thin-film gold, an electrical conductivity measurement (by the Van der Paaw method) was performed on 150nm Au deposited on an electrically insulating substrate, and the thermal conductivity was obtained by the Wiedmann-Franz law to be 110±2 W/mK, in excellent agreement with the experimental results reported here.

As reported here, the thermal exchange radius and thermal contact resistance values are smaller for higher thermal conductivity materials than for the samples with thermal conductivity between 0.36 and 1.1 W/mK. The general trend of observing a smaller thermal exchange radius with a larger value of sample thermal conductivity has been reported in finite element studies under limited probe configurations, and in contact with the sample[15]. Although the correlation does not appear to be very strong, the high thermal conductivity calibration seems to indicate that there may be a non-negligible dependence of R^{th}_C on sample thermal conductivity. If this is the case, the phenomenon may be explained by the probe geometry near the tip, since R^{th}_C is due mainly to air conduction between tip and sample[15]. As b increases, due the "V" shape of the Wollaston wire, the average distance between the probe and sample increases and thus the thermal contact resistance increases as well. By employing the calibration method developed in this work, practitioners will be able to find the contact parameters for their relevant thermal conductivity range.

3. Conclusions/Summary

We have observed that the assumption that the thermal exchange radius and thermal contact resistance are constant is valid for a certain range of sample thermal conductivity (0.36-1.1 W/K·m), which was achieved by measuring several bulk samples with known thermal conductivity that range, and plotting the thermal contact resistance as a function of thermal exchange radius, as well as by developing a separate method of calibration by measuring the Seebeck voltage and thermal resistance of a sample with known thermal conductivity and Seebeck coefficient. This yielded the same result as the intersection calibration method for low thermal conductivity samples within the margin of uncertainty. Above the lower thermal conductivity range, a separate calibration by intersection was performed, from which another pair of values of thermal contact resistance and thermal exchange radius was obtained, and was used to find the thermal conductivity of thin-film gold on glass, which matched previously published results, and independent measurement within margin ofuncertainty. The specifics of how the thermal exchange parameters vary with sample thermal conductivity remain unknown. However, this work shows that the experimental method may be suited for use for a wider range of thermal conductivity than what had previously been considered the range of validity, given that the calibration of thermal exchange parameters is performed in the appropriate range. It has also been established that given a film thickness and sample thermal properties such that the film may be treated as a semi-infinite medium, equation 5 may be used to find sample thermal conductivity and that for samples with small thickness, where substrate effects are non-negligible, multi-layered analytical heat conduction models must be employed to solve for the thermal conductivity. In this way, measurements on films of arbitrary thickness and of a wide range of thermal conductivity may be achieved.

Acknowledgements

We gratefully acknowledge funding from the US Department of Energy, Office of Basic Energy Sciences through the S3TEC Energy Frontiers Research Center (T.B.T.), and NSF IRES grant #1028071 for financial support towards this work (A.A.W. and D.B.T.). We would also like to acknowledge support from ECR StG NanoTEC 240497, and projects PHOMENTA MAT2011-27911 and NanoHiTEC project FP7-263306 (M.M.G.), and CSIC for a JAE Pre-Doctoral fellowship (M.M.R.).

Notes

[a] Department of Mechanical, Aerospace and Nuclear Engineering, Rensselaer Polytechnic Institute, 110 8th Street, Troy, NY 12180 USA

[b] Instituto de Microelectrónicas de Madrid, Consejo Superior de Investigaciones Científicas, Calle de Isaac Newton, 8, Tres Cantos, Madrid 28760, Spain

†Denotes corresponding author

Electronic Supplementary Information (ESI) available: SEM images from which probe geometry was found, determination of probe TCR, voltage distribution of 2ω Seebeck voltage on Sb-doped Bi_2Te_3, and how film thermal conductivity is found for samples with 2D heat spreading. See DOI: 10.1039/b000000x/

References

Nanoscale Accepted Manuscript

1 S. Ghosh, I. Calizo, D. Teweldebrhan, E. P. Pokatilov, D. L. Nika, A. A. Balandin, W. Bao, F. Miao, and C. N. Lau, *Appl. Phys. Lett.*,2008, **92**, 15.
2 L.E. Bell, *Science*, 2008, **321**, 5895.
3 T. C. Harman, P. J. Taylor, M. P. Walsh, and B. E. LaForge, *Science*, 2002, **297**, 5590.
4 S. B. Riffat and X. Ma, *Appl. Therm. Eng.*, 2003, **23**, 8.
5 J. L. Battaglia, A. Kusiak, C. Rossignol, and N. Chigarev, *J. Phys. Conf. Ser.*, 2007, **92**, 012083.
6 A. Rosencwaig and A. Gersho, *J. Appl. Phys.*, 1976, **47**, 1.
7 W. J. Parker, R. J. Jenkins, C. P. Butler, and G. L. Abbott, *J. Appl. Phys.*, 1961, **32**, 9.
8 S. E. Gustafsson, *Rev. Sci. Instrum.*, 1991, **62**, 3.
9 K. E. Goodson and M. I. Flik, *Appl. Mech. Rev.*, 1994, **47**, 3.
10 T. Borca-Tasciuc, D. A. Borca-Tasciuc, and G. Chen, *IEEE Trans. Components Packag. Technol.*, 2007, **30**, 4.
11 T. Borca-Tasciuc, *Annu. Rev. Heat Transf.*, 2013, **16**, 16.
12 M. Muñoz Rojo, S. Grauby, J. M. Rampnoux, O. Caballero-Calero, M. Martin-Gonzalez, and S. Dilhaire, *J. Appl. Phys.*, 2013, **113**, 5.
13 M. Muñoz Rojo, J. Martín, S. Grauby, T. Borca-Tasciuc, S. Dilhaire, and M. Martin-Gonzalez, *Nanoscale*, 2014, **6**, 14.
14 M. Muñoz Rojo, O.C. Calero, A. F. Lopeandia, J. Rodriguez-Viejo, and M. Martín-González. *Nanoscale,* 2013, **5**, 11526
15 S. Lefèvre, S. Volz, and P. O. Chapuis, *Int. J. Heat Mass Transf.*, 2006, **49**, 1–2.
16 Y. Zhang, C. L. Hapenciuc, E. E. Castillo, T. Borca-Tasciuc, R. J. Mehta, C. Karthik, and G. Ramanath, *Appl. Phys. Lett.*, 2010, **96**, 6.
17 Y. Zhang, E. E. Castillo, R. J. Mehta, G. Ramanath, and T. Borca-Tasciuc, *Rev. Sci. Instrum.*, 2011, **82**, 2.
18 E. Puyoo, S. Grauby, J. M. Rampnoux, E. Rouvière, and S. Dilhaire, *Rev. Sci. Instrum.*, 2010, **81**, 7.
19 E. Puyoo, S. Grauby, J. M. Rampnoux, E. Rouvière, and S. Dilhaire, *J. Appl. Phys.*, 2011, **109**, 2.
20 S. Lefèvre and S. Volz, *Rev. Sci. Instrum.*, 2005, **76**, 3.
21 K. Kim, W. Jeong, W. Lee, S. Sadat, D. Thompson, E. Meyhofer, and P. Reddy, *Appl. Phys. Lett.*, 2014, **105**, 20.
22 Y. Son, S. K. Pal, T. Borca-Tasciuc, P. M. Ajayan, and R. W. Siegel, *J. Appl. Phys.*, 2008, **103**, 2.
23 S. Gomes, N. Trannoy, P. Grossel, and F. Depasse, *Int. J. Therm. Sci.*, 2001, **40**, 01.
24 B. Abad, I. Alda, P. Díaz-Chao, H. Kawakami, A. Almarza, D. Amantia, D. Gutierrez, L. Aubouy, and M. Martín-González, *J. Mater. Chem. A*, 2013, **1**, 35.
25 K. H. Wu, C. I. Hung, P. Ziolkowski, D. Platzek, G. Karpinski, C. Stiewe, and E. Mueller, *Rev. Sci. Instrum.*, 2009, **80**, 10.
26 B. Abad, M. Rull-Bravo, S. Hodson, X. Xu, and M. Martín-González. *Electrochimica Acta,* 2015, **169**, 1.
27 T. Borca-Tasciuc, and G. Chen, *Int. J. Thermophys.*, 1998, **19**, 2.
28 G. Langer, J. Hartmann, and M. Reichling, *Rev. Sci. Instrum.*, 2001, **68**, 3.
29 S. Lefevre, S. Volz, J.B. Saulnier, and C. Fuentes. *Rev. Sci. Instrum.*, 2003, **74**, 4.
30 S. Lefevre, J. Saulnier, C. Fuentes, and S. Volz. *Superlattices and Microstructures,* 2004, **35**, 3-6.
31 D. Cahill. *J. Vac. Sci. & Tech.,* 1989, **7**, 3.
32 J. Schomacker. FEA Modelling of Heat Transfer Between a Joule Heated Wollaston Probe and Substrate [*master's thesis*]. [Troy, NY] Rensselaer Polytechnic Institute; 2014.

Nanoscale Accepted Manuscript

 This journal is © The Royal Society of Chemistry 2015